2-20-1997

# Partitioning of the reactive nitrogen reservoir in the lower sratosphere of the southern hemisphere: Observations and modeling

R. S. Gao
*National Oceanic and Atmospheric Administration*

D. W. Fahey
*National Oceanic and Atmospheric Administration*

R. J. Salawitch
*Jet Propulsion Laboratory*

S. A. Lloyd
*Johns Hopkins University*

D. E. Anderson
*Johns Hopkins University*

*See next page for additional authors*

JOURNAL OF GEOPHYSICAL RESEARCH, VOL. 102, NO. D3, PAGES 3935-3949, FEBRUARY 20, 1997

# Partitioning of the reactive nitrogen reservoir in the lower stratosphere of the southern hemisphere: Observations and modeling

R. S. Gao,[1,2] D. W. Fahey,[1] R. J. Salawitch,[3] S. A. Lloyd,[4] D. E. Anderson,[4] R. DeMajistre,[4] C. T. McElroy,[5] E. L. Woodbridge,[6] R. C. Wamsley,[1,2] S. G. Donnelly,[1,2] L. A. Del Negro,[1,2,7] M. H. Proffitt,[1,2] R. M. Stimpfle,[8] D. W. Kohn,[8] S. R. Kawa,[9] L. R. Lait,[9] M. Loewenstein,[10] J. R. Podolske,[10] E. R. Keim,[1,2] J. E. Dye,[11] J. C. Wilson,[12] and K. R. Chan[10]

**Abstract.** Measurements of nitric oxide (NO), nitrogen dioxide ($NO_2$), and total reactive nitrogen ($NO_y = NO + NO_2 + NO_3 + HNO_3 + ClONO_2 + 2N_2O_5 + ...$) were made during austral fall, winter, and spring 1994 as part of the NASA Airborne Southern Hemisphere Ozone Experiment/Measurements for Assessing the Effects of Stratospheric Aircraft mission. Comparisons between measured $NO_2$ values and those calculated using a steady state (SS) approximation are presented for flights at mid and high latitudes. The SS results agree with the measurements to within 8%, suggesting that the kinetic rate coefficients and calculated $NO_2$ photolysis rate used in the SS approximation are reasonably accurate for conditions in the lower stratosphere. However, $NO_2$ values observed in the Concorde exhaust plume were significantly less than SS values. Calculated $NO_2$ photolysis rates showed good agreement with values inferred from solar flux measurements, indicating a strong self-consistency in our understanding of UV radiation transmission in the lower stratosphere. Model comparisons using a full diurnal, photochemical steady state model also show good agreement with the NO and $NO_2$ measurements, suggesting that the reactions affecting the partitioning of the $NO_y$ reservoir are well understood in the lower stratosphere.

## Introduction

Stratospheric ozone ($O_3$) is destroyed in catalytic cycles involving oxides of hydrogen ($HO_x = OH + HO_2$), nitrogen ($NO_x = NO + NO_2$), chlorine ($ClO_x = Cl + ClO + 2ClOOCl$), and bromine ($BrO_x = Br + BrO$). Our understanding of $O_3$ destruction cycles changed significantly with the recognition of the role of heterogeneous reactions in the stratosphere [*Solomon et al.*, 1986; *McElroy et al.*, 1986, 1992; *Rodriguez et al.*, 1991; *Fahey et al.*, 1993; *Kolb et al.*, 1995; *Hanson et al.*, 1996]. On sulfate aerosol surfaces, the reactions

$$N_2O_5 + H_2O \xrightarrow{\text{aerosol}} 2HNO_3 \quad (1)$$

$$ClONO_2 + H_2O \xrightarrow{\text{aerosol}} HOCl + HNO_3 \quad (2)$$

$$BrONO_2 + H_2O \xrightarrow{\text{aerosol}} HOBr + HNO_3 \quad (3)$$

reduce the concentrations of $NO_x$ within the total reactive nitrogen ($NO_y = NO + NO_2 + NO_3 + HNO_3 + ClONO_2 + 2N_2O_5 + ...$) reservoir with nitric acid ($HNO_3$) product molecules released back into the gas phase. Since the abundance of $NO_x$ also controls the partitioning between the hydroxyl radical (OH) and hydroperoxyl radical ($HO_2$) and between chlorine monoxide (ClO) and chlorine nitrate($ClONO_2$), these heterogeneous reactions strongly influence the $O_3$ destruction rate [*Cohen et al.*, 1994; *Stimpfle et al.*, 1994; *Wennberg et al.*, 1994]. With the resulting increase in $HO_x$ and $ClO_x$ concentrations, the net contribution to $O_3$ loss from the $HO_x$, $ClO_x$, and $BrO_x$ catalytic cycles generally exceeds that of $NO_x$ in the lower stratosphere. Midlatitude measurements of species in each radical family have confirmed this hierarchy in the catalytic cycles [*Salawitch et al.*, 1994a; *Wennberg et al.*, 1994]. Figure 1 illustrates the relation of reactions (1) through (3) to other photochemical reactions that affect the partitioning of $NO_y$

[1]Aeronomy Laboratory, National Oceanic and Atmospheric Administration, Boulder, Colorado.
[2]Cooperative Institute for Research in Environmental Science, University of Colorado, Boulder.
[3]Jet Propulsion Laboratory, Pasadena, California.
[4]Applied Physics Laboratory, Johns Hopkins University, Laurel, Maryland.
[5]Atmospheric Environment Service/Canada, Downsview, Ontario.
[6]Scripps Institution of Oceanography, University of California at San Diego, La Jolla.
[7]Department of Chemistry and Biochemistry, University of Colorado, Boulder.
[8]Department of Chemistry, Harvard University, Cambridge, Massachussetts.
[9]NASA Goddard Space Flight Center, Greenbelt, Maryland.
[10]NASA Ames Research Center, Moffett Field, California.
[11]Mesoscale and Microscale Meteorology Division, National Center for Atmospheric Research, Boulder, Colorado.
[12]Department of Engineering, University of Denver, Colorado.



Paper number 96JD01967.
0148-0227/97/96JD-01967$09.00

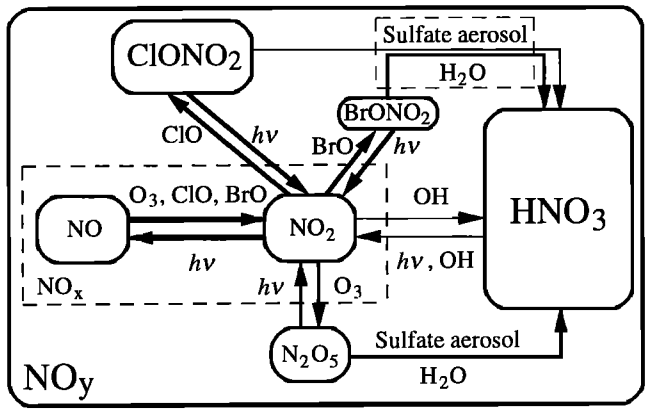


**Figure 1.** Diagram denoting the principal species of the $NO_y$ reservoir and reaction pathways relevant to the lower stratosphere. Larger boxes and thicker arrows indicate a greater abundance and larger reaction rate, respectively. Photolysis is designated as *hν*.

species. Although it generally constitutes less than 10% of the $NO_y$ reservoir, $NO_x$ plays a pivotal role in establishing the abundance of the other $NO_y$ component species.

Few stratospheric in situ measurements of nitrogen dioxide ($NO_2$) were made before 1994 [*Helten et al.*, 1984, 1985; *Hastie and Miller*, 1985; *McFarland et al.*, 1986; *Ridley et al.*, 1988; *Carroll et al.*, 1990; *Folkins et al.*, 1994], and not many of them include simultaneous measurements of $NO_y$. The most extensive in situ observations of reactive nitrogen made in the lower stratosphere include only measurements of nitric oxide (NO) and $NO_y$ [*Fahey et al.*, 1993; *Kondo et al.*, 1992]. Our understanding of the partitioning of $NO_y$ gases is facilitated by examining the $NO_x/NO_y$ ratio, since the concentration of NO and $NO_2$ changes by large amounts during the day due primarily to changes in solar radiation, while the concentration of $NO_x$ is nearly constant over a diurnal cycle. Past studies of the role of reactions (1) through (3) on $NO_y$ partitioning, for example, have relied on estimating the $NO_x/NO_y$ ratio using concentrations of $NO_2$ calculated from simultaneous measurements of NO, $O_3$, ClO, and theoretical values for the photolysis rate of $NO_2$, assuming steady state (SS) concentrations of NO and $NO_2$ [*Webster*, 1987; *Kawa et al.*, 1990, 1992]. Recent in situ measurements of $NO_2$ together with NO and $NO_y$ made in the lower stratosphere during the 1993 NASA Stratospheric Photochemistry, Aerosol, and Dynamics Expedition (SPADE) provided an opportunity to test directly our understanding of the $NO_x/NO_y$ ratio and the partitioning of NO and $NO_2$ [*Gao et al.*, 1994; *Jaeglé et al.*, 1994]. The concentrations of $NO_2$ from the Jet Propulsion Laboratory (JPL) Aircraft Laser IR Absorption Spectrometer (ALIAS) instrument and the National Oceanic and Atmospheric Administration (NOAA) Aeronomy Laboratory instrument used here were approximately 40% lower than SS abundances calculated with simultaneous measurements of NO, $O_3$, and ClO [*Jaeglé et al.*, 1994; *Salawitch et al.*, 1994b]. However, the uncertainties are ~20% and 60%, respectively, for the JPL and NOAA $NO_2$ measurements and ~60% for inferred $NO_2$ values. (The largest contribution to this uncertainty is from the reaction rate of NO + $O_3$). Consequently, the significance of the discrepancy between observation and theory for the $NO/NO_2$ ratio suggested by the SPADE observations remains unclear.

The NASA Airborne Southern Hemisphere Ozone Experiment/Measurements for Assessing the Effects of Stratospheric Aircraft (ASHOE/MAESA) mission was conducted in California, Hawaii, Fiji, and New Zealand from February to November 1994. Poleward flights (45°S to 68°S) by the NASA ER-2 high-altitude aircraft from Christchurch repeatedly reached the edge region of the Antarctic vortex throughout its lifetime. Simultaneous measurements of NO, $NO_2$, and $NO_y$ are available from 10 ASHOE/MAESA flights, along with more than 20 other measurements of trace gases, radicals, aerosols, the solar radiation field, and meteorological parameters. Important improvements made to the NOAA Aeronomy Laboratory $NO_2$ detector between the SPADE and ASHOE/MAESA missions have reduced significantly the systematic errors in the $NO_2$ measurements. The combined ER-2 measurement set includes values of the photolysis rate of $NO_2$ ($J_{NO2}$) from solar radiometer observations (on four flights), from an SS expression incorporating the trace gas observations (on all 10 flights) and from radiation scattering models. The calculation of SS $NO_2$ is performed using two of these independent $J_{NO2}$ values. Comparisons are presented for both modeled and measured values of $J_{NO2}$ and $NO_2$. The extensive ASHOE/MAESA data set also provides a unique opportunity to test our understanding of the partitioning within the $NO_y$ reservoir over an extended time period in the lower stratosphere. Using 4 of the 10 flights, we present measured NO, $NO_2$ (three of four flights), and the $NO_x/NO_y$ ratio from austral autumn to spring and compare these values to SS $NO_2$ values and the results from a photochemical stationary state model (PSS). Since no ALIAS $NO_2$ measurements were made during ASHOE/MAESA, comparisons similar to those made with SPADE data cannot be repeated here.

## Measurements

The reactive nitrogen species NO, $NO_2$, and $NO_y$ are measured with a three-channel chemiluminescence detector (CLD) on the ER-2 aircraft (Figure 2) [*Fahey et al.*, 1989, 1993; *Gao et al.*, 1994]. In the first CLD channel, NO is detected in an air sample using the chemiluminescence reaction with reagent $O_3$. The resultant excited-state $NO_2$ molecule subsequently relaxes to the ground state, emitting an infrared photon. A photomultiplier monitors the photons emitted by $NO_2$ molecules, providing a signal proportional to the ambient NO concentration. $NO_y$ detection is achieved by using a gold catalytic converter upstream in the second CLD channel sample line. The catalytic converter reduces $NO_y$ molecules to NO. For $NO_2$ detection a UV photolysis system located in the sample line of the third CLD channel is used to convert ~50% of $NO_2$ to NO with a sample residence time of 1 s. Measured NO is then the sum of ambient NO and NO produced from photolysis of ambient $NO_2$. The latter is determined by subtracting the ambient NO signal using values obtained simultaneously in the first channel.

When the $NO_2$ photolysis system was first operated during the SPADE mission [*Gao et al.*, 1994], uncertainties in the $NO_2$ measurements were dominated by the UV-induced artifact. This artifact occurs in the photolysis system when UV radiation used to photodissociate $NO_2$ releases NO or $NO_2$ from the wall of the cell in reactions involving other $NO_y$ species. The most likely source of the earlier artifact is $HNO_3$ photolysis from short-wavelength (< 340 nm) UV radiation transmitted into

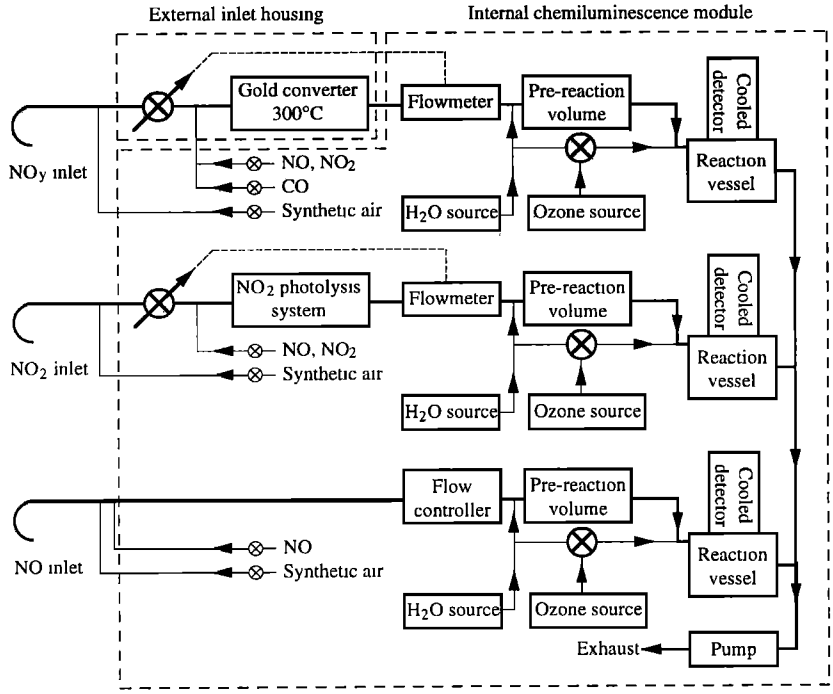


**Figure 2a.** Schematic of the NOAA Aeronomy Laboratory $NO_y$ chemiluminescence detector. The internal chemiluminescence module resides inside the ER-2 fuselage (Figure 2b). The NO, $NO_y$, and $NO_2$ external inlets are located approximately 48, 48, and 25 cm below the fuselage, respectively. See *Fahey et al.* [1989] and *Gao et al.* [1994] for more detailed descriptions.

the photolysis cell, producing NO or $NO_2$. Since the $HNO_3$ concentration is at least an order of magnitude higher than that of $NO_2$ in the lower stratosphere, the photolysis of even a small fraction of $HNO_3$ can be a severe interference. During SPADE the $NO_2$ uncertainties of ~30 to 60% were primarily from the UV artifact. The largest sources of uncertainty in the present $NO_2$ measurements are (1) the UV artifact, (2) the subtraction of the ambient NO signal from the $NO_2$ channel response, and (3) the instrument background. However, in the current configuration the addition of a long-pass optical filter to the photolysis system has virtually eliminated the interference from $HNO_3$ as determined in laboratory tests. In flight the remaining UV artifact was checked periodically using the addition of synthetic air to the sample flow [*Gao et al.*, 1994]. Typical values of ~0.1 part per billion by volume (ppbv) were constant throughout a flight and comparable to those measured in the laboratory. Measurements of the artifact, photolytic conversion fraction of $NO_2$ to NO, and instrument background are obtained regularly throughout each flight and incorporated directly into the data reduction algorithm used to calculate the $NO_2$ mixing ratio.

The accurate subtraction of the ambient NO signal from the $NO_2$ channel signal relies on the assumption that NO is detected equivalently in both channels. As stated by *Gao et*

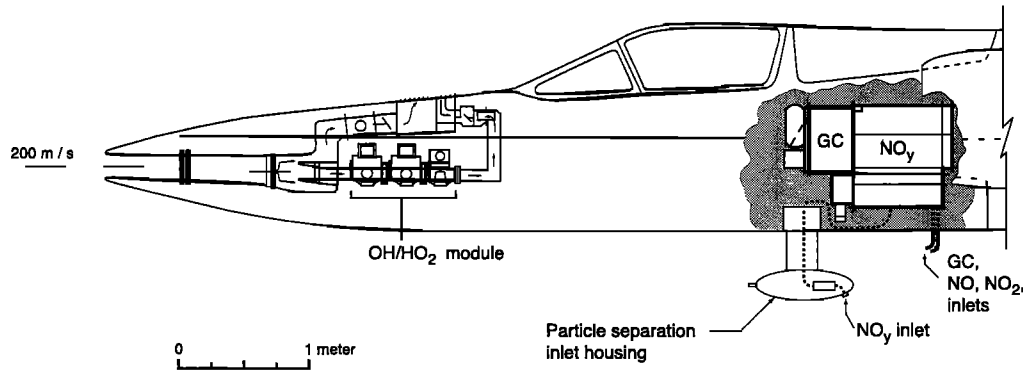


**Figure 2b.** Schematic of the forward fuselage of the ER-2 high-altitude aircraft showing the location of the reactive nitrogen ($NO_y$), gas chromatograph (GC) [*Elkins et al.*, 1996], and OH and $HO_2$ instruments [*Wennberg et al.*, 1995]. The $NO_y$ inlet is shown at the rear of the external housing designed for particle separation. The $NO_2$ photolysis module is located in the lower forward section of the $NO_y$ enclosure. The inlets for NO and $NO_2$ are mounted on the fuselage directly below the instrument. Addition of calibration gas to the sample lines occurs inside the fuselage for NO and $NO_2$ and inside the external housing upstream of the catalyst for $NO_y$.

*al.* [1994], in-flight checks during SPADE revealed that NO values from the NO channel were always 10% higher than from the $NO_2$ channel when the photolysis lamp was off. This difference persisted throughout the ASHOE/MAESA mission. Although the difference was corrected in the NO subtraction, a significant error is associated with this step. This error now represents the largest source of uncertainty in $NO_2$ measurements at midlatitudes where ambient NO concentrations typically exceed those of $NO_2$. Ambient $NO_2$ concentrations at high latitudes during polar winter are usually greater than those of NO, while $NO_x$ concentrations are usually lower than at midlatitudes. At high latitudes the uncertainty associated with the instrument background predominates over other error sources. Overall, a systematic error estimate of ±20 to 30% applies when $NO_2$ mixing ratios are above 0.1 ppbv and $NO_2$/NO ratios are above unity and thus covers virtually all $NO_2$ data presented in this paper.

Another potential artifact source in the $NO_2$ measurement is the thermal decomposition of $ClONO_2$, $N_2O_5$, and $HO_2NO_2$ combined with the photolysis of decomposition products to form NO. Gas phase decomposition fractions depend on the temperature and residence time of the photolysis cell and inlet lines [*Gao et al.*, 1994]. For typical cell conditions (12°C and 1.1 s) associated with the data presented here, the respective gas phase decomposition fractions are all less than 1%. However, heterogeneous decomposition could further increase the artifact response. In-flight tests conducted to examine the effect of these decomposition processes in a system with higher cell temperatures and longer residence times were inconclusive [*Carroll et al.*, 1990]. The comparison of the ratio of measured to SS $NO_2$ values presented below is less than unity on average (0.92 ± 0.14) over a range of estimated $ClONO_2$, $N_2O_5$, and $HO_2NO_2$ values, thereby offering some evidence that $NO_y$ interferences are not significant.

Solar irradiance between 300 and 775 nm was measured on the ER-2 with the Composition and Photodissociative Flux Measurement (CPFM) instrument [*McElroy*, 1995]. Using the wavelength-dependent flux data, the photodissociation rate of $NO_2$ as well as of other molecules can be derived [*McElroy et al.*, 1995]. Values of $J_{NO2}$ are typically in the range of 0.01 to 0.02 $s^{-1}$ for solar zenith angles (SZA) less than 80°. In the ASHOE/MAESA data set, $J_{NO2}$ values from the CPFM instrument are available for the four flights where $NO_2$ measurements are also available. The uncertainties associated with the CPFM $J_{NO2}$ values of ~15% include the non-Lambertian cloud-scattering effect which leads to an overestimation of total scattered light.

The SS calculations and PSS model described below utilize the concentration of radicals and trace molecules, aerosol properties, and meteorological parameters measured by other instruments aboard the ER-2 during ASHOE/MAESA. Uncertainties associated with measured quantities are provided in Table 1.

**Table 1.** ER-2 Instrument Characteristics

| Measurement | Accuracy, ± σ[a] | Sample Period, s | Reference |
|---|---|---|---|
| NO | 15% | 1 | *Fahey et al.* [1989] |
| $NO_2$ | 20-30% | 1 | *Gao et al.* [1994] |
| $NO_y$ | 15% | 1 | *Fahey et al.* [1989] |
| $O_3$ | 5% | 1 | *Proffitt et al.* [1989b] |
| BrO | 20% | 3600 | *Brune et al.* [1989a] |
| ClO | 15% | 16 | *Brune et al.* [1989b] |
| $J_{NO2}$ | 15% | 164 | *McElroy et al.* [1995] |
| Pressure | 0.5 mbar | 1 | *Scott et al.* [1990] |
| Temperature | 0.3K | 1 | *Scott et al.* [1990] |
| Aerosols | < 100% | 10 | *Jonsson et al.* [1995]<br>*Baumgardner et al.* [1996] |

[a]Systematic error estimates.

## SS Calculations

The basic reactions controlling the $NO_2$/NO ratio in the lower stratosphere are

$$NO + O_3 \rightarrow NO_2 + O_2 \quad (4)$$
$$NO + ClO \rightarrow NO_2 + Cl \quad (5)$$
$$NO + BrO \rightarrow NO_2 + Br \quad (6)$$
$$NO_2 + h\nu \rightarrow NO + O \quad (7)$$

where the reaction of $HO_2$ + NO can be ignored. The combined time constant of reactions (4) through (7) is of the order of 100 s in the lower stratosphere when the SZA is less than 85° [*DeMore et al.*, 1994]. Under this condition the assumption that NO and $NO_2$ are in photochemical steady state is valid; hence $NO_2$ can be expressed as

$$[NO_2] = \frac{[NO](k_{NO+O_3}[O_3] + k_{NO+ClO}[ClO] + k_{NO+BrO}[BrO])}{J_{NO_2}} \quad (8)$$

where brackets indicate species concentrations and $k$ values are rate coefficients [*DeMore et al.*, 1994]. The contribution of the BrO term, $k_{NO+BrO}$[NO][BrO], is sometimes neglected. In the ASHOE/MAESA data set, a compact correlation exists between the extensive measurements of BrO and CFC-11 (both at low time resolution, >> 1 s). Using the observed correlation, the data set of $N_2O$ measurements at higher time resolution (1 s) and a similar compact correlation between $N_2O$ and CFC-11, the bromine monoxide (BrO) mixing ratio is estimated for each 1-s point along the ER-2 flight track [*Woodbridge et al.*, 1995].

In addition to the $J_{NO2}$ values derived from the solar irradiance measurements, two sets of theoretical $J_{NO2}$ values were calculated independently for the ER-2 flight track. Both were calculated with isotropic, spherical, multiple-scattering models of the atmospheric radiation field and incorporate wavelength-dependent photolysis cross sections for $NO_2$ [*Prather*, 1981; *Anderson et al.*, 1995]. Both models used values of UV reflectivity (a surrogate for albedo) and total $O_3$ from the Total Ozone Mapping Spectrometer (TOMS) to calculate specific J values along the flight track. The wavelength-dependent transmission calculated by both models has been compared extensively as part of the 1995 Scientific Assessment of the Atmospheric Effects of Stratospheric Aircraft photolysis benchmark [*Stolarski et al.*, 1995]. Values from the two calculations show excellent agreement. For simplicity, only one set (based on *Prather* [1981] and used by *Salawitch et al.* [1994a, b]) is used in the SS and PSS model calculations and $J_{NO2}$ comparisons in this work. The uncertainty associated with modeling $J_{NO2}$ is estimated to be 30% based on comparable uncertainties for the radiative flux and $NO_2$ absorption cross section [*Jaeglé et al.*, 1994].

## PSS Model Calculations

The PSS model is used in this work to calculate the steady state abundances of a variety of reactive species at ~15-min

intervals throughout a 24-hour period by balancing the production and loss of each species integrated over a diurnal cycle [*Salawitch et al.*, 1994a, b]. Since the steady state solution includes the explicit diurnal variation of each species, detailed comparisons can be made to in situ observations along the ER-2 flight track by selecting model results for the corresponding local time. The PSS calculations use pressure, temperature, and latitude of air parcels encountered by the ER-2; measured concentrations of $NO_y$, $O_3$, water ($H_2O$), methane ($CH_4$), and aerosol surface area; and concentrations of inorganic chlorine ($Cl_y$) and inorganic bromine ($Br_y$) inferred from observed relations between chlorofluorocarbons [*Woodbridge et al.*, 1995] and brominated source gases [*Salawitch et al.*, 1994a; *Schauffler et al.*, 1993], respectively. Aerosol surface area values were obtained from the Focused Cavity Aerosol Spectrometer (FCAS), which detects the number concentration of particles with diameters between 0.06 and 2 μm [*Jonsson et al.*, 1995], and from the Multiple-Angle Aerosol Spectrometer Probe (MASP), which observes particles with diameters between 0.2 and 20 μm [*Baumgardner et al.*, 1996]. With the decay of aerosol loading since the Mount Pinatubo eruption in 1991, these diameter ranges include essentially all of the surface area of the background aerosol distribution.

The PSS model includes 35 reactive species and ~220 chemical reactions, with most reaction rates and absorption cross sections adopted from *DeMore et al.* [1994]. A reaction probability of 0.1 was used for the heterogeneous hydrolysis of $N_2O_5$ (R1). A reaction probability of 0.5 was used for the heterogeneous reaction of $BrONO_2 + H_2O$ (R3), based on recent laboratory measurements by *Hanson and Ravishankara* [1995]. The formulation of *Hanson and Ravishankara* [1994] and *Hanson et al.* [1994] were used for the rates of the heterogeneous reaction set $ClONO_2 + H_2O$ (R2) and $ClONO_2$ + HCl, and the heterogeneous reaction of hypochlorous acid (HOCl) and hydrogen chloride (HCl), respectively. Heterogeneous reactions involving HCl have a negligible effect on model results for temperatures encountered on these flights, except for certain poleward regions on the flight of August 6, 1994, as discussed below. The *Michelsen et al.* [1994] model, which allows for the photolysis of vibrationally and rotationally excited $O_3$, was used to calculate the quantum yields of the first excited state of atomic oxygen ($O(^1D)$) from $O_3$ photolysis. Finally, absorption cross sections for hydrogen peroxide ($H_2O_2$), nitrous acid (HONO), and peroxynitric acid ($HNO_4$) were extrapolated to longer wavelengths than in the work of *DeMore et al.* [1994] for a more accurate accounting of the photolysis of these gases at high SZA.

A Newton-Raphson iterative technique was used to find the set of diurnally varying species concentrations that repeats every 24 hours, thereby satisfying the criterion that production and loss for each species, integrated over a diurnal cycle, are equal [*Logan et al.*, 1978]. The photochemical lifetimes (mean concentrations divided by the integrated production rate) are <<1 day for $HO_x$, ~1 week for $NO_x$, and ~1 month for HCl. If before sampling by the ER-2, an air parcel has undergone excursions in either temperature or latitude that exceeds 10 K or 15°, respectively, then the PSS calculations may not be valid [*Kawa et al.*, 1993]. $NO_x$ concentrations are especially sensitive to temperature and latitude history; OH is much less sensitive. A comparison of temperature and latitude of air parcels sampled by the ER-2 with the 10-day history of temperature and latitude, calculated using a trajectory model, is important for understanding where the PSS model may not be expected to provide a good simulation of $NO_x$.

## Results and Discussion

### NO and $NO_2$

The average volume mixing ratios of measured NO and $NO_2$ for each of the 10 flights are listed in Table 2. Results for

**Table 2.** Comparison of $NO_2$ Mixing Ratios Between Measurements and Steady State Calculations

| Flight[b] | Latitude Coverage | SZA, deg | Data,[c] hours | Measurements NO, ppbv | Measurements $NO_2$, ppbv | $NO_2$ Steady State Calculation[a] Using Measured $J_{NO_2}$, ppbv[d] | Measured/ Calculated[e] | Using Calculated $J_{NO_2}$, ppbv[f] | Measured/ Calculated[e] |
|---|---|---|---|---|---|---|---|---|---|
| 940214 | 37.5°N - 40.2°N | 50° - 54° | 0.7 | 0.17 | 0.19 | 0.21 | 0.90±0.10 | 0.20 | 0.93±0.16 |
| 940218 | 38.0°N - 60.8°N | 62° - 73° | 3.5 | 0.09 | 0.17 | 0.20 | 0.86±0.20 | 0.20 | 0.87±0.23 |
| 940318 | 22.9°N - 36.7°N | 24° - 46° | 2.0 | 0.40 | 0.30 | 0.30 | 0.99±0.07 | 0.34 | 0.91±0.07 |
| 940330 | 46.5°S - 66.6°S | 55° - 80° | 3.0 | 0.18 | 0.19 | 0.19 | 0.98±0.07 | 0.21 | 0.92±0.16 |
| **Average (4 flights)** | | | | | | | **0.94±0.14** | | **0.90±0.10** |
| 940601 | 45.3°S - 60.9°S | 70° - 85° | 1.4 | 0.08 | 0.12 | | | 0.12 | 1.0±0.21 |
| 941008 | 40.1°S - 42.5°S | 43° - 65° | 1.0 | 0.15 | 0.14 | | | 0.16 | 0.91±0.14 |
| 941010 | 45.1°S - 70.0°S | 51° - 67° | 4.3 | 0.20 | 0.35 | | | 0.38 | 0.92±0.11 |
| 941013 | 43.8°S - 68.3°S | 47° - 70° | 4.4 | 0.19 | 0.34 | | | 0.38 | 0.91±0.09 |
| 941016 | 45.0°S - 69.5°S | 45° - 58° | 4.3 | 0.18 | 0.41 | | | 0.41 | 0.99±0.11 |
| 941020 | 46.5°S - 64.0°S | 52° - 65° | 3.1 | 0.29 | 0.37 | | | 0.41 | 0.90±0.09 |
| **Average (10 flights)** | | | | | | | | | **0.92±0.14** |

[a]Equation (8) is used for the steady state calculation.
[b]Read 940214 as February 14, 1994.
[c]Total combined length of data record used in flight.
[d]$J_{NO_2}$ derived from measurements made by the Composition and Photodissociative Flux Measurement instrument.
[e]Average is calculated as $\left(\sum_n \frac{\text{measured } NO_2}{\text{calculated } NO_2}\right)/n$ where $n$ is the number of 100-s averaged data points. Averages are shown with ±1σ standard deviation.
[f]$J_{NO_2}$ calculated by *Salawitch et al.* [1994a, b].

individual flights are shown in Figures 3 and 4, with related measurements displayed in Figures 5 and 6. Average NO values are generally 0.2 ppbv or lower, with comparable or higher $NO_2$ values. SS $NO_2$ values from equation (8) were derived using theoretically calculated $J_{NO_2}$ values and those from the solar radiation measurements. Measurements and calculations corresponding to SZA > 85° are excluded from Table 2. Measurements made in the Concorde plume on October 8, 1994, discussed in more detail below, also are excluded. Although no other data filtering is applied, most of the values correspond to pressures between 50 and 100 mbar (ER-2 cruise altitudes) in the lower stratosphere. The ratio of measured $NO_2$ to SS $NO_2$ values is averaged for individual as well as for all 10 flights. As shown in Table 2, good agreement exists between the measurements and the calculations, with no evidence of a seasonal or latitudinal dependence. The average measured $NO_2$ value is lower than the calculated SS values (equation (8)) by 8% . Excluding the NO + BrO reaction (not shown in Table 2) decreases the discrepancy to 5%. Thus the NO + BrO reaction, as the least important of the three loss processes for NO in equation (8), usually can be neglected in the lower stratosphere. Using solar $J_{NO_2}$ values to calculate SS $NO_2$ appears to produce slightly better agreement than theoretical $J_{NO_2}$ values, but the difference is much less than the uncertainties in both measurements and calculations.

The differences between measured and SS $NO_2$ values are significantly smaller than those found using the SPADE observations and less than the current experimental uncertainties (Table 1). The number of observations and the seasonal and latitudinal range of the data greatly exceed that of the SPADE data set. The primary $NO_2$ observations made during SPADE were obtained by the ALIAS instrument, which utilizes tunable diode laser absorption spectroscopy [*Jaeglé et al.*, 1994]. Using the SPADE comparison, SS $NO_2$ values have been reduced by a factor of 0.7 in other interpretive studies [*Wennberg et al.*, 1994]. On the basis of the ASHOE/MAESA results presented here, we do not recommend adjusting SS $NO_2$ values either by increasing $J_{NO_2}$ values (as calculated from the radiation scattering models used here) or by reducing the NO + $O_3$ (R4) reaction rate constant, both of which are required to calculate the $NO_2$/NO ratio in the lower stratosphere.

## Concorde Observations

On October 8, 1994, the ER-2 instruments sampled the exhaust plume of a Concorde supersonic passenger aircraft *in the lower stratosphere [Fahey et al.*, 1995a]. $NO_x$ observations in several plume encounter events showed values to be well above background values. In the plume, NO and $NO_2$ reach steady state (equation (8)) within a few minutes with near-ambient concentrations of $O_3$, whereas the age of the exhaust at the time of sampling ranged from 10 to 60 min. For an age of 16 min, Figure 7 shows the comparison of measured and SS $NO_2$ values, where the expected good agreement was found outside the plume (Table 2). Inside the plume, however, peak values calculated for $NO_2$ are a factor of 2 higher than measured values. Furthermore, the sum of NO and SS $NO_2$ integrated inside the plume is ~10% higher than measured $NO_y$. Similar results were found as the plume age increased. Although instrumental issues cannot be completely ruled out, the most likely source of the discrepancy is that the SS expression (equation (8)) must be modified to account for other important reactions in the plume. For example, constituent species present only in the plume may react with $NO_2$ to form NO. The reaction may occur in the gas phase or may be a heterogeneous process involving the large number of aerosol particles observed in the plume [*Fahey et al.*, 1995a]. Alternatively, an increased abundance of aerosols in the plume may cause an increase in the effective value of $J_{NO_2}$. However, the $J_{NO_2}$ enhancement needed to account for the data is larger than could be reasonably expected, based on calculations using a scattering model that describes the effect of aerosols on the radiation field. The consistency of the $O_3$-$N_2O$ correlation through the plume encounters and the high dilution of the plume ($10^5$) indicates that $O_3$ values are free of artifacts in the plume and are essentially equal to ambient values. In an earlier study of the ER-2 plume [*Fahey et al.*, 1995b], measurements were obtained at night when NO is absent and no subtraction of the ambient NO signal is required to obtain an $NO_2$ value. In this case, the $NO_x/NO_y$ ratio was 0.80, similar to values found in other plumes sampled during daylight. Thus $NO_2$ loss during sampling or other instrumental issues are unlikely to account for all of the discrepancy in the Concorde observations. At this point, the present data set is not sufficient to resolve this issue.

## $J_{NO_2}$ Values

The steady state value of $J_{NO_2}$ can be expressed by rearranging equation (8) to yield

$$J_{NO_2} = \frac{[NO](k_{NO+O_3}[O_3] + k_{NO+ClO}[ClO] + k_{NO+BrO}[BrO])}{[NO_2]} \quad (9)$$

Equation (9) allows $J_{NO_2}$ values that are self-consistent with reactive trace species observations (chemical) to be compared with $J_{NO_2}$ values inferred from the CPFM flux measurements (solar) or values calculated from a radiation transfer model (theoretical). The total measurement uncertainty in these chemically derived $J_{NO_2}$ values (Figure 8) is estimated by propagating errors in the associated measurements (Table 1), assuming that there is no correlation of errors between individual measurements [*Bevington*, 1969]. Results shown in Figure 8 for the flight on March 18, 1994, show that the agreement between values of $J_{NO_2}$ from the three methods is well within the measurement uncertainties at midlatitudes.

The chemical and solar values of $J_{NO_2}$ derived from ER-2 measurements show more variability than the radiative-transfer model values. The model calculations rely on the TOMS satellite for both total column $O_3$ along the flight path and, more importantly, the effective UV reflectivity at a climatologically derived cloud height. Since the effective nadir footprint in the TOMS satellite data set is ~150 km, variability of the radiation field on small spatial scales is not resolved. Hence a model incorporating these data will not represent the subgrid scale variability of the real atmosphere. Work is currently in progress to correlate the abundance of species with a short photolytic lifetime (specifically OH and NO) with the variability of the radiation field observed by the CPFM instrument.

## NOy partitioning

During ASHOE/MAESA, four ER-2 deployments were based in Christchurch, New Zealand, between March and October 1994. In each deployment, three or four ER-2 flights were made poleward of Christchurch reaching 65°-68°S latitude.

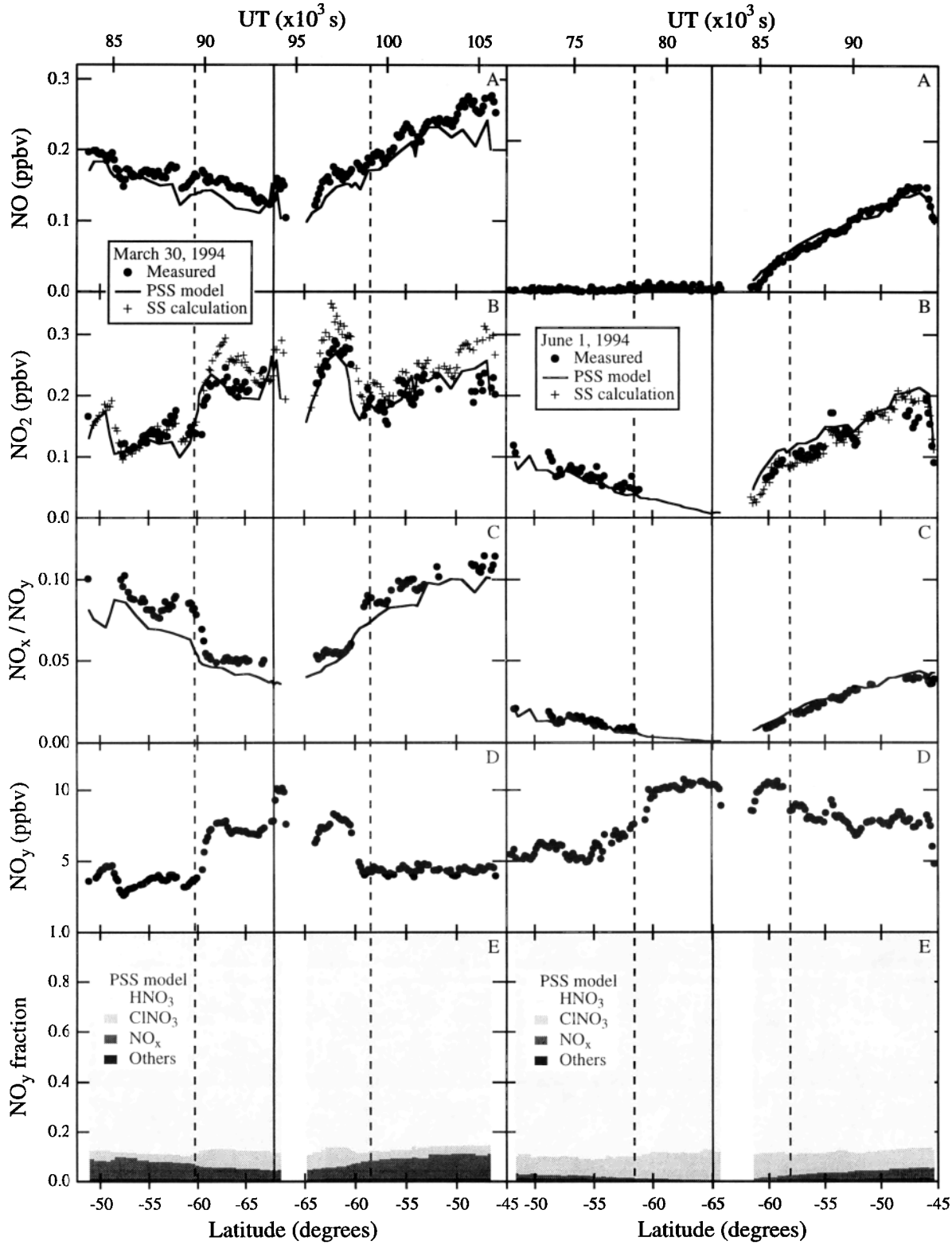


**Figure 3.** NO, $NO_2$, $NO_x/NO_y$, and $NO_y$ mixing ratios measured on March 30 and June 1, 1994, are shown in panels A, B, C, and D, respectively (solid circles). The top axis represents universal time (UT) along the flight track and the bottom axis represents the approximate latitude in the southern hemisphere. Values for $NO_2$ from the steady state (SS) approximation (equation (8)) are shown in panel B (open diamonds). Measured and SS values are averaged over 100 s along the flight track (20 km). The photochemical steady state (PSS) model results are shown in panels A - D (solid lines) and in panel E. A pressure filter of 53-73 mbar (altitude range of 18.2-20.2 km) is applied to all results presented here. The vertical solid line in the middle of flight panel indicates the southernmost point of the flight track from Christchurch. The two dashed lines represent a reference point for the edge of the Antarctic vortex.

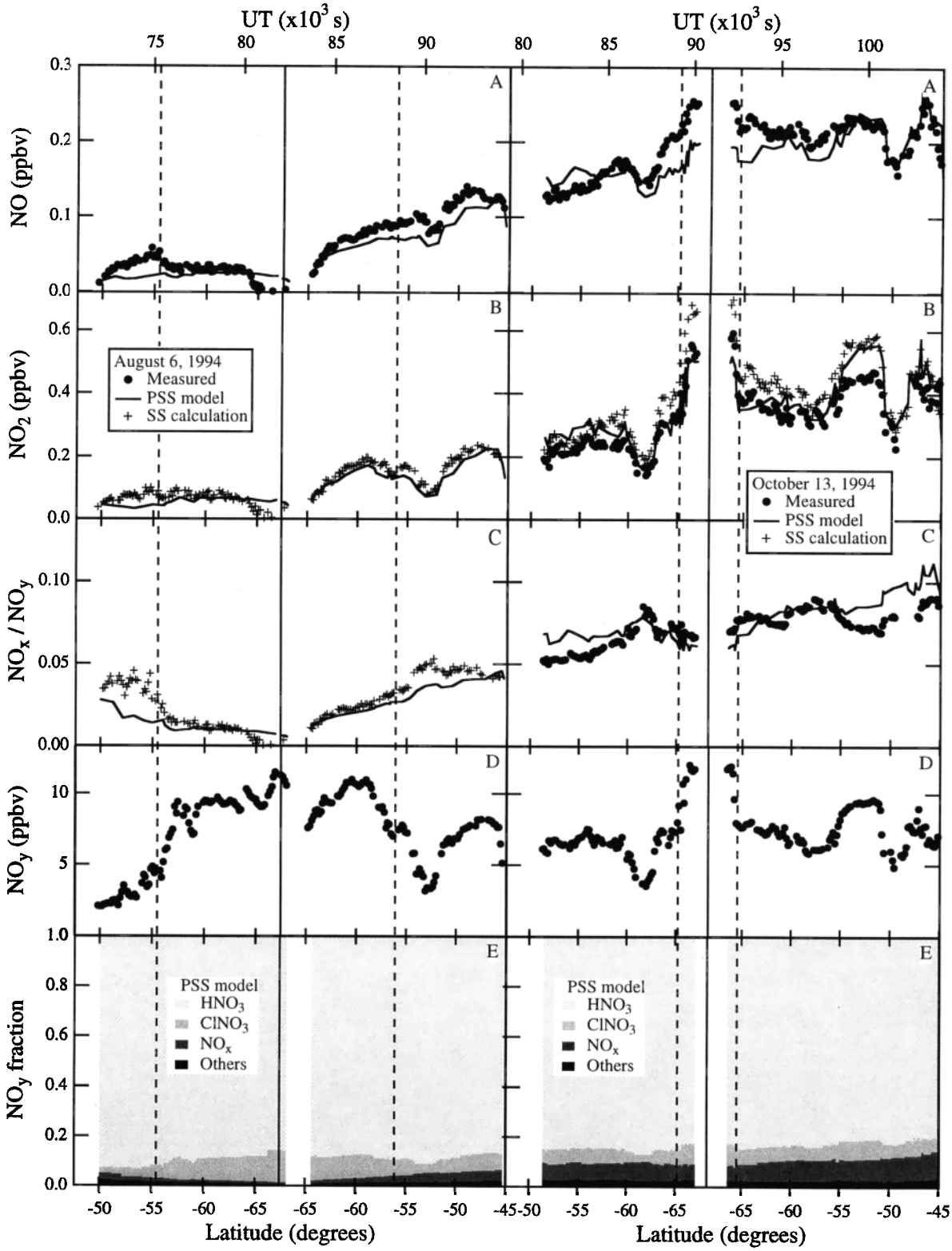


**Figure 4.** Measurements and model results for the flights of August 6 and October 13, 1994. Other details are the same as for Figure 3.

The flights were clustered in periods of about two weeks. Four flights (March 30, June 1, August 6, and October 13), one from each deployment, were chosen for a detailed evaluation of the partitioning within the $NO_y$ reservoir. The flights of March 30 and June 1 were chosen because of the availability of $NO_2$ measurements (compare Table 2). No $NO_2$ measurements are available for the late winter (July-August) deployment. However, the flight of August 6 was chosen because of interesting features in the measurements of other species, as discussed below. Since $NO_2$ measurements are available for all

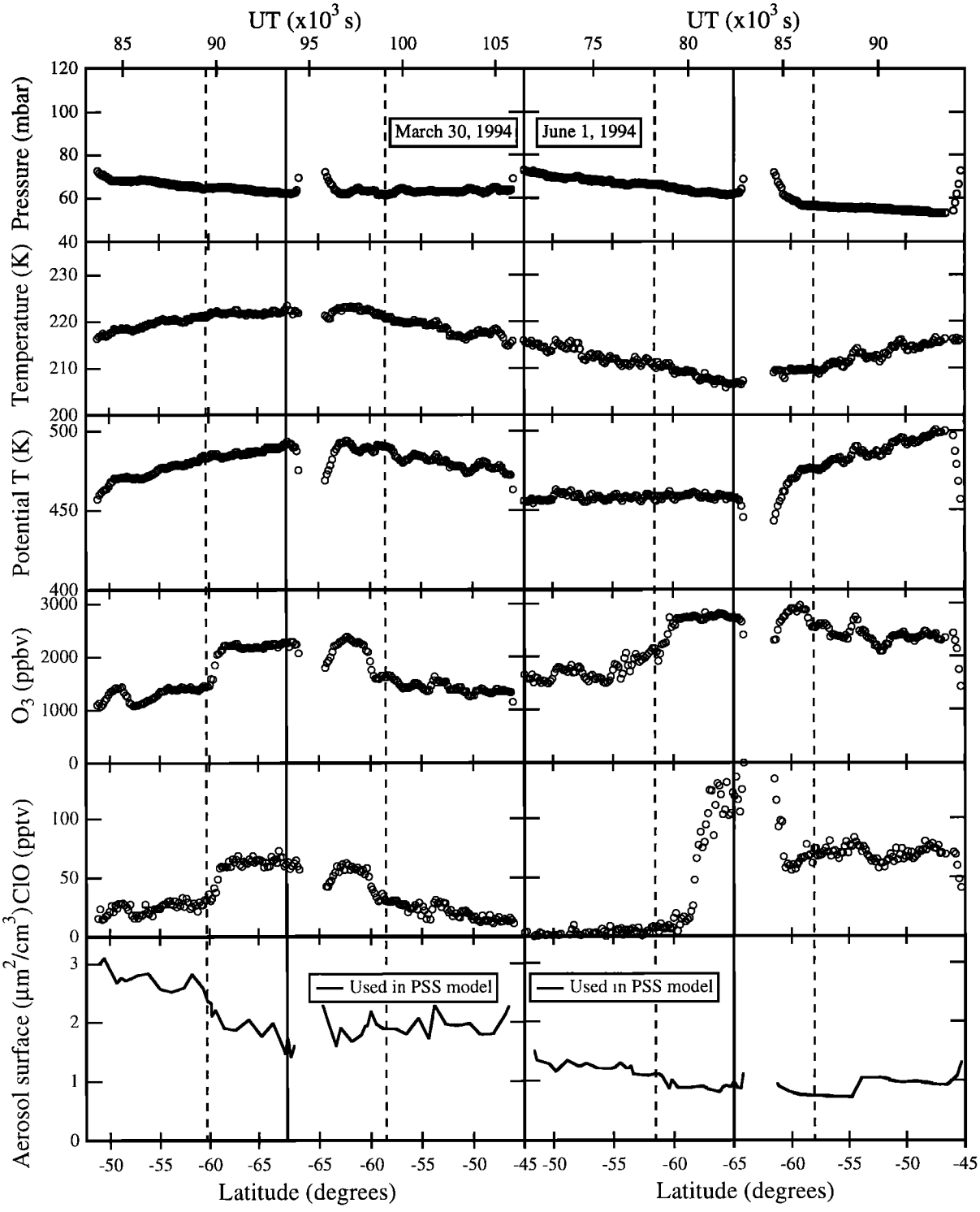


**Figure 5.** Related parameters and measurements made by other ER-2 instruments on March 30 and June 1, 1994, and used in the PSS model calculations. Aerosol values are estimated using the correlation with $N_2O$ obtained on other flights in the March and June time periods.

poleward flights in October, one flight (October 13) was chosen to be representative. For each flight, measured values of NO, $NO_2$, $NO_y$, and $NO_x/NO_y$ are plotted as a function of latitude in Figures 3 and 4. Also shown are $NO_2$ values from the SS approximation, using theoretically calculated $J_{NO_2}$, and NO and $NO_2$ values from the PSS model calculations. Finally, the PSS results for the fraction of $NO_y$ attributed to $HNO_3$, $ClONO_2$, and $NO_x$ are shown as a histogram. Data are shown only for ER-2 cruise conditions in the lower stratosphere (pressures between 53 and 73 mbar). The solid line in the middle of each figure indicates the poleward limit of each flight. A dashed line indicates a reference location in the

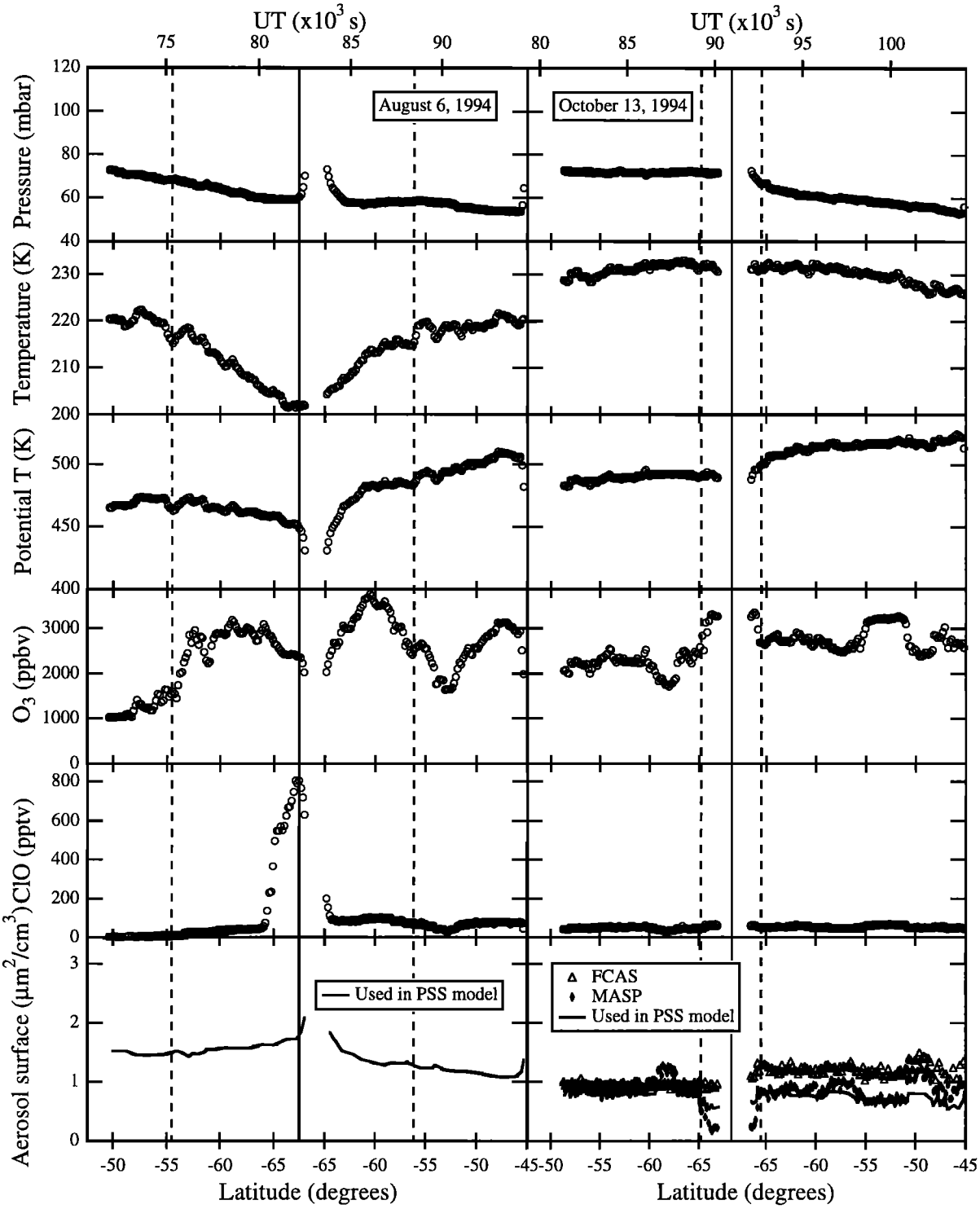


**Figure 6.** Related parameters and measurements made by other ER-2 instruments on August 6 and October 13, 1994, and used in the PSS model calculations. Aerosol surface area measurements (symbols) on October 13 include those of the Focused Cavity Aerosol Spectrometer (FCAS) [*Jonsson et al.*, 1995] and Multiple-Angle Aerosol Spectrometer Probe (MASP) [*Baumgardner et al.*, 1996] instruments. The line in the aerosol panel represents values estimated using the correlation with $N_2O$ obtained on other flights in the August and October time periods.

vortex edge region on each flight leg. The location marks the latitude where the difference between the equatorward and the poleward horizontal wind gradients (after heavy smoothing) is a maximum. As shown in Figures 5 and 6, this wind-gradient reference coincides fairly consistently with sharp changes in the horizontal gradients of $NO_y$ and $O_3$. Other choices of a reference location are the onset of highly enhanced ClO (> 0.15 ppbv) due to polar stratospheric cloud (PSC) processing [*Proffitt et al.*, 1989a] and the maximum in the horizontal wind [*Kawa et al.*, 1992]. Neither of these definitions yield

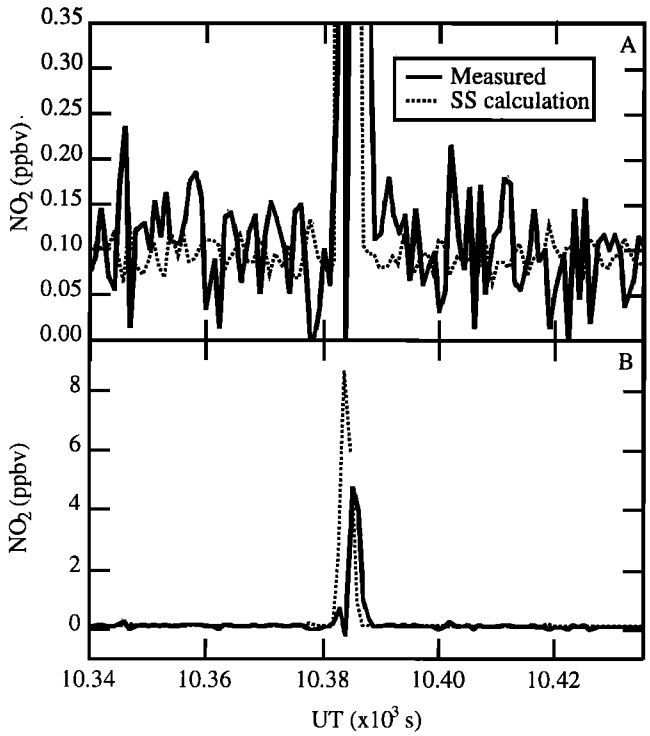


**Figure 7.** Segment of $NO_2$ measurements (1-s sample period) made on the Concorde plume sampling fight of October 8, 1994. Data are plotted as a function of UT along the ER-2 flight track. In the top panel, the vertical scale is expanded around a plume event to highlight measurements (solid line) and SS values (dashed line) (equation (8)) outside the plume. The bottom panel shows the increase in $NO_2$ that occurs when the Concorde plume is encountered. The time delay and change in shape noted between the measured and the SS $NO_2$ peaks is caused by the difference in residence time in the NO and $NO_2$ sample lines (see Figure 2). These differences do not affect the comparison of $NO_2$ values if integrated peak areas are used.

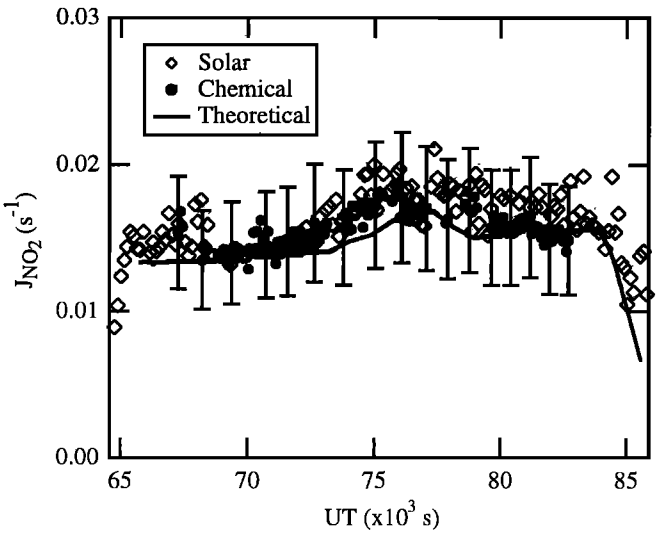


**Figure 8.** Values of $J_{NO2}$ for the flight of March 18, 1994. "Solar" values (open diamonds) are derived from solar irradiance measurements by the Composition and Photodissociative Flux Measurement instrument. "Chemical" values are derived from equation (9) using NO, $NO_2$, $O_3$, ClO, and BrO observations and averaged over 100 s (solid circles with error bars representing the total error propagated from individual measurement uncertainties). "Theoretical" values are those calculated using an atmospheric radiation-scattering model (solid line). The estimated uncertainty of the solar and theoretical values is ±15% and ±30%, respectively (see text).

consistent results for the data presented here, particularly because high ClO values are absent in nonwinter seasons (Figures 5 and 6).

Other ER-2 measurements used in the SS and PSS calculations are shown in Figures 5 and 6. Aerosol surface area measurements are not available for the first three flights due to various instrumental issues. Instead, values are estimated using the relation between aerosol and $N_2O$, an excellent tracer of air motion, obtained in flights preceding and following these three flights. Because the aerosol perturbations from the 1991 Mount Pinatubo eruption have decayed significantly, the aerosol surface area varies smoothly along the flight tracks. Specifically, aerosol surface areas in the lower stratosphere were in the range 1 to 5 $\mu m^2$ $cm^{-3}$ during 1994 (*J. C. Wilson et al.*, manuscript in preparation, 1996), having decreased from peak values of 20 to 100 $\mu m^2$ $cm^{-3}$ [*Wilson et al.*, 1993] following the Mount Pinatubo eruption.

NO and $NO_2$ values are both bounded by 0.3 ppbv for observations obtained in March and June 1994 (Figure 3) and by 0.3 and 0.6 ppbv, respectively, during August and October 1994 (Figure 4). For the three flights with $NO_2$ measurements, good agreement is found between measured and SS $NO_2$ values, as shown in Figures 3 and 4 and in Table 2. $NO_x/NO_y$ values vary from 0.01 to 0.1, with the lowest values found in winter (for August 6, SS $NO_2$ is used to infer $NO_x/NO_y$ in the absence of $NO_2$ observations). The agreement between observed abundances of NO, $NO_2$, and $NO_x/NO_y$ and theoretical values found using the PSS model is also generally very good. PSS model results shown in the histogram panels of Figures 3 and 4 indicate that $HNO_3$ is expected to constitute more than 80% of the $NO_y$ reservoir for the range of $NO_y$ (2 to 11 ppbv) and $O_3$ (1 to 4 ppmv) sampled during the four flights. The next most abundant species are expected to be $NO_x$ and $ClONO_2$, with other species such as $N_2O_5$ consistently constituting less than a few percent of the $NO_y$ reservoir. The flight on June 1 is of special interest because the first half occurred in the dark (SZA > 92°) (Figure 3). As expected, both observed and calculated values of NO are zero since NO is converted to $NO_2$ in the absence of sunlight. The SS approximation (equation (8)) is not applicable in the dark because $J_{NO2}$ equals zero. However, the PSS model, constrained in part by measured $NO_y$, simulates all components of the $NO_y$ family throughout a 24-hour period. The agreement of the PSS results for $NO_2$ with values observed prior to local sunrise increases confidence in our theoretical understanding of the diurnal variation of $NO_y$ species.

As illustrated in Figure 1, $NO_2$ is a key species in the $NO_y$ reservoir because it is reactively coupled to $N_2O_5$ which, following hydrolysis on sulfate aerosols (equation (1)), provides a reactive sink for $NO_x$. Furthermore, the reaction of $NO_2$ with oxygen atoms controls $O_3$ removal by $NO_y$ species [*Wennberg et al.*, 1994]. An accurate simulation of measured $NO_2$ concentrations must include a realistic representation of

the photolysis field and the reaction kinetics for many other species, including OH, $N_2O_5$, and $HNO_3$. Thus the ability of the PSS model to accurately simulate observed $NO_2$ levels for the range of conditions in Figures 3 and 4 demonstrates confidence in our understanding of the effect of heterogeneous reactions on $NO_y$ partitioning and the impact of $NO_y$ gases on $O_3$ removal rates, and in the calculated concentrations of a wide range of other species.

On the August 6 flight, NO values approached zero inside the vortex edge region, poleward of 65°S (Figure 4). Although no $NO_2$ observations are available for this flight, SS $NO_2$ values are also low. High ClO mixing ratios found in this region (Figure 6) indicate that $NO_x$ values must be low because of enhanced $ClONO_2$ formation. In this region, PSS values for NO and $NO_2$ are significantly larger than observed NO and SS $NO_2$ values, respectively. The associated air parcels, although at temperatures above those required for PSC formation, probably underwent recent processing by PSCs that led to enhanced ClO concentrations. Back trajectory calculations show that some of the air parcels reached temperatures as low as 192 K (Figure 9) in the preceding 10 days. For these air parcels the photochemical steady state assumption is not valid, because high concentrations of ClO decay over a period of days to weeks after exposure to PSCs. The decay is controlled through the formation of $NO_2$ from $HNO_3$ photolysis and reaction with OH and through the reaction of $NO_2$ with ClO to reform $ClONO_2$. Thus the balance among $NO_x$, $ClONO_2$, and $HNO_3$ cannot be simulated accurately for these air parcels unless heterogeneous processing by PSCs is estimated using a separate model that includes the recent temperature and latitude history of air parcels. *Kawa et al.* [1996] and *Jaeglé et al.* (Evolution and stoichiometry of heterogeneous processing in the Antarctic stratosphere, submitted to *Journal of Geophysical Research*, 1996) demonstrate good agreement among observations of $NO_x$, $ClO_x$, and $HO_x$ radicals and simulations using trajectory models for air parcels that have undergone recent exposure to PSCs.

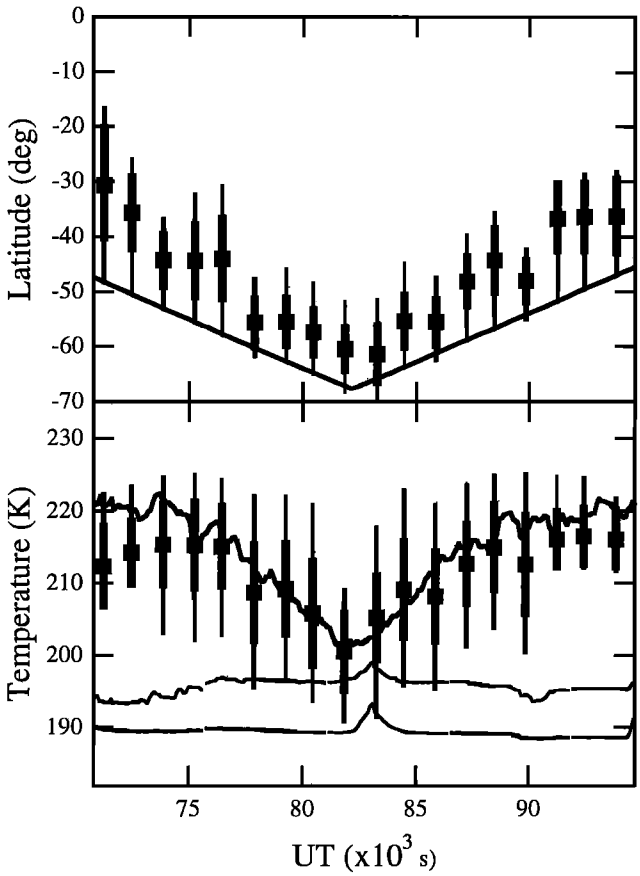


**Figure 9.** Results of 10-day back trajectory calculations for the flight on August 6, 1994, showing (top) latitudinal positions and (bottom) temperature. Continuous curves in each panel show flight track observations. The two lower curves in the bottom panel indicate approximate threshold temperatures for nitric acid trihydrate (upper) and ice aerosol (lower) formation. The individual points represent the mean (square), standard deviation (thick vertical line), and extrema (thin vertical line) in the trajectory values obtained during the 10 days prior to sampling at each point along the flight track.

For another portion of the 6 August flight (outbound leg, 50°S to 60°S), observed values of $NO_x/NO_y$ and theoretical values from the PSS model differ by a factor of 2 or more, where observed $NO_x$ is defined here as the sum of measured NO and SS $NO_2$. As discussed above, such differences are expected when air parcels experience recent latitude excursions of more than 15°. Indeed, 10-day back trajectory calculations indicate that these air parcels experienced latitudinal movement as large as 20° (Figure 9). In these extreme cases the PSS calculations represent a limit for observed $NO_x$ values. When the recent movement is poleward, toward lower average insolation, PSS values for $NO_2$ and NO are expected to be lower than observed values. This expectation is consistent with the comparison between theory and observation outside the vortex on August 6 (Figure 4). *Kawa et al.* [1993] found that for one high-latitude case, good agreement between theory and observation for NO required using a photochemical model that accounted for the variations of latitude and temperature during the last 10 days. In general, smaller-latitude excursions of 10° or less are not expected to lead to noticeable discrepancies.

The low $NO_x/NO_y$ levels during winter (1 June and 6 August) are the combined result of heterogeneous reactions on aerosol particle surfaces, higher $O_3$ concentrations, and low average insolation. The heterogeneous reactions (1) to (3) on sulfate aerosol have been demonstrated in the laboratory [*Tolbert et al.*, 1988; *Hanson and Ravishankara*, 1991; *Van Doren et al.*, 1991; *Hanson et al.*, 1996] and have been inferred from observations [*McElroy et al.*, 1992; *Keys et al.*, 1993; *Fahey et al.*, 1993; *Toon et al.*, 1993; *Koike et al.*, 1993, 1994]. The lowest measured value of the $NO_x/NO_y$ ratio, shown in Figure 3 for 1 June, is ~0.01. The related value of $NO_x$ is near the detection limit of the chemiluminescence detectors. These direct measurements confirm previous studies that inferred the presence of low $NO_x/NO_y$ values in the winter polar vortices [*Fahey et al.*, 1990; *Kawa et al.*, 1993]. As an illustration of the effect that heterogeneous processes have on partitioning the $NO_y$ reservoir, heterogeneous reaction rates were set to zero in the PSS model. The results, expressed as the ratio of $NO_x$ calculated using only gas phase chemistry to that using both heterogeneous and gas phase chemistry, are shown in Figure 10 for 1 June. The large values of this ratio demonstrate the importance of heterogeneous chemistry for regulating $NO_y$ partitioning in the winter polar regions.

The latitudinal and seasonal dependence of the $NO_x/NO_y$ and $ClONO_2/NO_y$ ratios calculated using the PSS model are shown in Figure 11. Only the return legs to Christchurch are shown

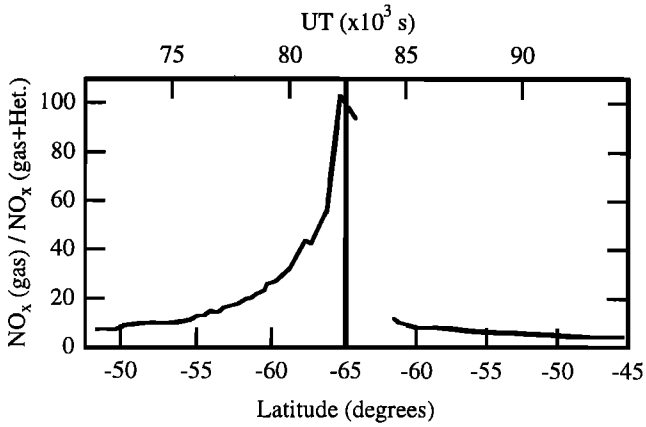


**Figure 10.** Ratio of $NO_x$ calculated using gas phase chemistry to that using both heterogeneous and gas phase chemistry from the PSS model results for the flight of June 1, 1994 for pressures between 53 and 73 mbar.

because the ambient pressure ranges were similar for each of the four flights (Figures 5 and 6). $NO_x/NO_y$ values, as discussed above, are reduced dramatically during winter, especially at the highest latitudes. However, in October (spring) the $NO_x/NO_y$ ratio returns to similar values found for March (fall) values. The $ClONO_2/NO_y$ ratio shows opposite changes with season, with larger values occurring in winter. However, values are still much higher for October than for March. The $ClONO_2/NO_y$ ratio shows more flight-to-flight variability than the $NO_x/NO_y$ ratio, as well as more variability within individual flights. The increased variability originates from the fact that model values for $ClONO_2/NO_y$ are constrained not only by measured $NO_y$ but also by total $Cl_y$ as observed from concentrations of chlorinated source gases. As illustrated in Figure 12, $Cl_y$ for the return legs of the four flights, as derived from $N_2O$ using the relation of *Woodbridge et al.* [1995], varied significantly within individual flights and from flight to flight.

## Conclusions

In situ measurements of NO, $NO_2$, and $NO_y$ have been obtained in the lower stratosphere of the southern hemisphere at midlatitudes and inside and near the edge of the Antarctic vortex. The measurements were made over multiweek periods in the fall, winter, and spring seasons as part of the 1994 ASHOE/MAESA campaign. $NO_2$ mixing ratio values were calculated using a steady state approximation (equation (8)) that incorporates simultaneous observations of NO, $O_3$, ClO, and BrO, and $J_{NO2}$ values calculated using a radiative transfer model. These calculated $NO_2$ values agree well with measured $NO_2$ values throughout the data set, except inside the Concorde exhaust plume where measured $NO_2$ values were significantly lower. Averaged over the 10 flights for which $NO_2$ observations are available, measured mixing ratios of

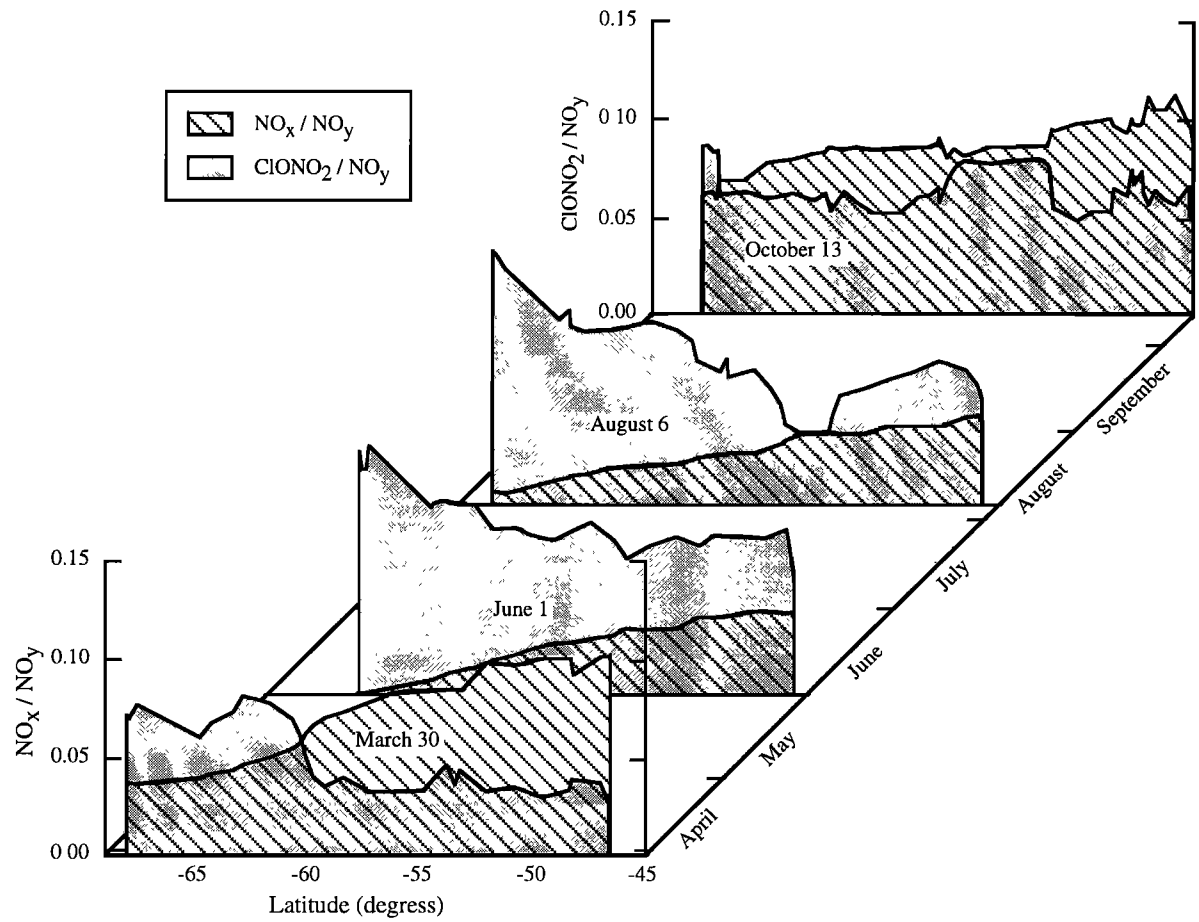


**Figure 11.** $NO_x/NO_y$ (striped) and $ClONO_2/NO_y$ (shaded) ratios from PSS model calculations shown as a function of time and latitude for the flights in Figures 3 and 4.

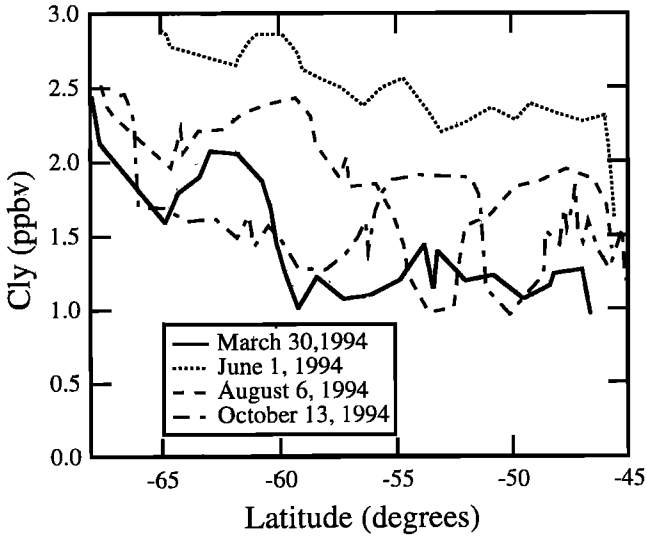


**Figure 12.** $Cl_y$ used in the PSS model calculations for the flights shown in Figures 3 and 4.

$NO_2$ are ~8% lower than calculated values. This difference is significantly smaller than the uncertainty of the measurements, and much less than the differences found in a similar comparison using data acquired during the SPADE campaign. On the basis of the comparisons presented here, we do not recommend any corrections to $J_{NO2}$ values calculated from the radiation scattering models or to the rate constants used in the steady state calculations.

Excellent agreement was found for $NO_2$ photolysis rates estimated three ways: derived from direct measurements of solar flux, inferred from measured concentrations of reactive species, and calculated using a radiative transfer model. The "solar" photolysis rate relies on in situ observations of the solar flux in the UV region and laboratory photodissociation cross sections for $NO_2$. The "chemical" rate is found using a steady state relation that incorporates in situ observations of concentrations of NO, $NO_2$, $O_3$, ClO, and BrO and laboratory reaction rate coefficients. The "theoretical" rate is obtained using a radiation scattering model with full spherical symmetry and multiple-scattering processes, constrained by satellite observations of total $O_3$ and UV reflectivity. The agreement of the "solar," "chemical," and "theoretical" rates of $NO_2$ photolysis indicates a strong self-consistency in our understanding of the transmission of UV radiation in the lower stratosphere, the influence of UV radiation on reactive species, and the kinetics of processes that partition NO and $NO_2$.

A full diurnal photochemical model simulation was also used for comparison to the NO and $NO_2$ observations. In general, the agreement between observation and theory for the $NO_x/NO_y$ ratio is excellent, with exceptions attributed to the absence of steady state conditions caused by recent PSC processing or large and rapid latitude excursions. Our observations show that the $NO_x/NO_y$ ratio is reduced significantly at high latitudes during winter and subsequently recovers in the spring, consistent with the previous in situ observations of NO and $NO_y$ [*Fahey et al.*, 1990; *Kawa et al.*, 1993]. As a result of the low observed $NO_x/NO_y$ ratios, $HNO_3$ is expected to comprise 80% or more of the $NO_y$ reservoir throughout mid to high latitudes in the lower stratosphere. The agreement of observation and theory for $NO_x/NO_y$ demonstrates that heterogeneous processes of sulfate aerosols regulate the partitioning of the $NO_y$ reservoir for a wide range of lower stratospheric conditions. Our results suggest that photochemical models properly constrained by observations and incorporating the latest kinetic values for gas phase and heterogeneous reaction rates as well as absorption cross sections are well suited to represent the partitioning within the $NO_y$ reservoir and the coupling to other reactive species.

**Acknowledgments.** This work was supported by the NASA High Speed Research Program and the Upper Atmosphere Research Program.

## References

Anderson, D. E., R. DeMajistre, S. A. Lloyd, and P. K. Swaminathan, Photodissociation in the troposphere and stratosphere· Radiation field models for clouds, aerosols, and twilight, *J. Geophys. Res., 100*, 7135-7145, 1995.

Baumgardner, D., J. E. Dye, B. Gandrud, K. Barr, K. K. Kelly, and K. R. Chan, Refractive indices of aerosols in the upper troposphere and lower stratosphere, *Geophys. Res. Lett., 23*, 749-752, 1996.

Bevington, P. R., *Data Reduction and Error Analysis for the Physical Sciences*, McGraw-Hill, New York, 1969.

Brune, W. H., J. G. Anderson, and K. R. Chan, In situ observations of BrO over Antarctica: ER-2 aircraft results from 54°S to 72°S latitude, *J. Geophys. Res., 94*, 16,639-16,647, 1989a.

Brune, W. H., J. G. Anderson, and K. R. Chan, In situ observations of ClO over Antarctica: ER-2 aircraft results from 54°S to 72°S latitude, *J. Geophys. Res., 94*, 16,649-16,663, 1989b.

Carroll, M. A., D. D. Montzka, G. Hübler, and K. K. Kelly, In situ measurements of $NO_x$ in the Airborne Arctic Stratospheric Expedition, *Geophys. Res. Lett., 17*, 493-496, 1990.

Cohen, R. C., et al., Are models of catalytic removal of $O_3$ by $HO_x$ accurate? Constraints from in situ measurements of the OH to $HO_2$ ratio, *Geophys. Res. Lett., 21*, 2539-2542, 1994.

DeMore, W. B., S. P. Sander, D. M. Golden, R. F. Hampson, M. J. Kurylo, C. J. Howard, A. R. Ravishankara, C. E. Kolb, and M. J Molina, Chemical kinetics and photochemical data for use in stratospheric modeling, *JPL Publ., 94-26*, Jet Propul. Lab., Pasadena, Calif., 1994.

Fahey, D. W., K. K. Kelly, G. V. Ferry, L. R. Poole, J. C. Wilson, D. M. Murphy, M. Loewenstein, and K. R. Chan, In situ measurements of total reactive nitrogen, total water, and aerosol in a polar stratospheric cloud in the Antarctic, *J. Geophys. Res., 94*, 11,299-11,315, 1989.

Fahey, D. W., S. R. Kawa, and K. R. Chan, Nitric oxide measurements in the Arctic winter stratosphere, *Geophys. Res. Lett., 17*, 489-492, 1990.

Fahey, D. W., et al., In situ measurements constraining the role of sulphate aerosols in mid-latitude ozone depletion, *Nature, 363*, 509-514, 1993.

Fahey, D. W., et al., Emission measurements of the Concorde supersonic aircraft in the lower stratosphere, *Science, 270*, 70-74, 1995a.

Fahey, D. W., et al., In situ observations in aircraft exhaust plumes in the lower stratosphere at midlatitudes, *J Geophys. Res., 100*, 3065-3074, 1995b

Folkins, I., A. J. Weinheimer, G. Brasseur, F. LeFèvre , B. A. Ridley, J. G. Walega, J. E. Collins, and R. F. Pueschel, Three-dimensional model interpretation of $NO_x$ measurements from the lower stratosphere, *J. Geophys. Res., 99*, 23,117-23,129, 1994.

Gao, R. S., E. R. Keim, E. L. Woodbridge, S. J. Ciciora, M. H. Proffitt, T. L. Thompson, R. J. McLaughlin, and D. W. Fahey, New photolysis system for $NO_2$ measurements in the lower stratosphere, *J. Geophys. Res., 99*, 20,673-20,681, 1994.

Hanson, D. R., and A. R. Ravishankara, The reaction probabilities of $ClONO_2$ and $N_2O_5$ on 40 to 75 percent sulfuric acid solutions, *J. Geophys. Res , 96*, 17,307-17,314, 1991.

Hanson, D. R., and A. R. Ravishankara, Reactive uptake of $ClONO_2$ onto sulfuric acid due to reaction with HCl and $H_2O$, *J. Phys. Chem, 98*, 5728-5735, 1994.

Hanson, D. R., A. R. Ravishankara, and S. Solomon, Heterogeneous reactions in sulfuric acid aerosols: A framework for model calculations, *J. Geophys. Res., 99*, 3615-3629, 1994.

Hanson, D. R., and A. R. Ravishankara, Heterogeneous chemistry of bromine species in sulfuric acid under stratospheric conditions, *Geophys. Res. Lett., 22*, 385-388, 1995.

Hanson, D. R., A. R. Ravishankara, and E. R. Lovejoy, Reaction of BrONO2 with $H_2O$ on submicron sulfuric acid aerosol and the implications for the lower stratosphere, *J. Geophys. Res., 101*, 9063-9069, 1996.

Hastie, D. R., and M. D. Miller, Balloon-borne tunable diode laser absorption spectrometer for multispecies trace gas measurements in the stratosphere., *Appl. Opt.*, *24*, 3694-3701, 1985.

Helten, M., W. Patz, M. Trainer, H. Fark, E. Klein, and D. H. Ehhalt, Measurements of stratospheric $HO_2$ and $NO_2$ by matrix isolation and ESR spectroscopy, *J. Atmos. Chem.*, *2*, 191-202, 1984.

Helten, M., W. Patz, D. H. Ehhalt, and E. P. Roeth, Measurements of nighttime $NO_3$ and $NO_2$ in the stratosphere by matrix isolation and ESR spectroscopy, in *Atmospheric Ozone*, edited by C. S. Zerefos and A. Ghazi, pp. 196-200, D. Reidel, Norwell, Mass., 1985.

Jaeglé, L., et al., In situ measurements of the $NO_2$/NO ratio for testing atmospheric photochemical models, *Geophys. Res. Lett.*, *21*, 2555-2558, 1994.

Jonsson, H. H., et al., Performance of a focused cavity aerosol spectrometer for measurements in the stratosphere of particle size in the 0.06-2.0 μm diameter range, *J. Atmos. Oceanic Tech.*, *12*, 115-129, 1995.

Kawa, S. R., D. W. Fahey, S. Solomon, W. H. Brune, M. H. Proffitt, D. W. Toohey, D. E. Anderson Jr., L. C. Anderson, and K. R. Chan, Interpretation of aircraft measurements of NO, ClO, and $O_3$ in the lower stratosphere, *J. Geophys. Res.*, *95*, 18,597-18,609, 1990.

Kawa, S. R., et al., Photochemical partitioning of the reactive nitrogen and chlorine reservoirs in the high-latitude stratosphere, *J. Geophys. Res.*, *97*, 7905-7923, 1992.

Kawa, S. R., et al., Interpretation of $NO_x/NO_y$ observations from AASE-II using a model of chemistry along trajectories, *Geophys. Res. Lett.*, *20*, 2507-2510, 1993.

Kawa, S. R., et al., Activation of chlorine in sulfate aerosol as inferred from aircraft observations, *J. Geophys. Res.*, this issue.

Keys, J. G., P. V. Johnston, R. D. Blatherwick, and F. J. Murcray, Evidence for heterogeneous reactions in the Antarctic autumn stratosphere, *Nature*, *361*, 49-51, 1993.

Koike, M., Y. Kondo, W. A. Matthews, P. V. Johnston, and K. Yamazaki, Decrease of stratospheric $NO_2$ at 44°N caused by Pinatubo volcanic aerosols, *Geophys. Res. Lett.*, *20*, 1975-1978, 1993.

Koike, M., N. B. Jones, W. A. Matthews, P. V. Johnston, R. L . McKenzie, D. Kinnison, and J. Rodriguez, Impact of Pinatubo aerosols on the partitioning between $NO_2$ and $HNO_3$, *Geophys. Res. Lett.*, *21*, 597-600, 1994.

Kolb, C. E., et al., Laboratory studies of atmospheric heterogeneous chemistry, in *Progress and Problems in Atmospheric Chemistry*, Edited by J. R. Barker, World Scientific Publishing, Singapore, 1995.

Kondo, Y., P. Aimedieu, M. Koike, Y. Iwasaka, P A. Newman, U. Schmidt, W. A. Matthews, M. Hayashi, and W. R. Sheldon, Reactive nitrogen, ozone, and nitrate aerosols observed in the Arctic stratosphere in January 1990, *J. Geophys. Res.*, *97*, 13,025-13,038, 1992.

Logan, J. A., M. J. Prather, S. C. Wofsy, and M. B. McElroy, Atmospheric chemistry: Response to human influence, *Philos. Trans. R. Soc. BA*, *290*, 187-234, 1978.

McElroy, C. T., A spectroradiometer for the measurement of direct and scattered solar irradiance from on-board the NASA ER-2 high-altitude research aircraft, *Geophys. Res. Lett.*, *22*, 1361-1364, 1995.

McElroy, C. T., C. Midwinter, D. V. Barton, and R. B. Hall, A comparison of J-values from the composition and photodissociative flux measurement with model calculations, *Geophys. Res. Lett.*, *22*, 1365-1368, 1995.

McElroy, M. B., R. J. Salawitch, S. C. Wofsy, and J. A. Logan, Reduction of Antarctic ozone due to synergistic interactions of chlorine and bromine, *Nature*, *321*, 759-762, 1986.

McElroy, M. B., R. J. Salawitch, and K. Minschwaner, The changing stratosphere, *Planet. Space Sci.*, *40*, 373-401, 1992.

McFarland, M., B. A. Ridley, M. H. Proffitt, D. L. Albritton, T. L. Thompson, W. J. Harrop, R. H. Winkler, and A. L. Schmeltekopf, Simultaneous in situ measurements of nitrogen dioxide, nitric oxide, and ozone between 20 and 31 km, *J. Geophys. Res.*, *91*, 5421-5437, 1986.

Michelsen, H. A., R. J. Salawitch, P. O. Wennberg, and J. G. Anderson, Production of $O(^1D)$ from photolysis of $O_3$, *Geophys. Res. Lett.*, *21*, 2227-2230, 1994.

Prather, M. J., Ozone in the upper stratosphere and mesosphere, *J. Geophys. Res.*, *86*, 5325-5338, 1981.

Proffitt, M. H., et al., A chemical definition of the boundary of the Antarctic ozone hole, *J. Geophys. Res.*, *94*, 11,437-11,448, 1989a.

Proffitt, M. H., et al., In situ ozone measurements within the 1987 Antarctic ozone hole from a high-altitude ER-2 aircraft, *J. Geophys. Res.*, *94*, 16,547-16,556, 1989b.

Ridley, B. A., M. A. Carroll, G. L. Gregory, and G. W. Sachse, NO and $NO_2$ in the troposphere: Technique and measurements within regions of a folded tropopause, *J. Geophys. Res.*, *93*, 15,813-15,830, 1988.

Rodriguez, J. M., M. K. W. Ko, and N. D. Sze, Role of heterogeneous conversion of $N_2O_5$ on sulphate aerosols in global ozone losses, *Nature*, *352*, 134-137, 1991.

Salawitch, R. J., et al., The distribution of hydrogen, nitrogen, and chlorine radicals in the lower stratosphere: Implications for changes in $O_3$ due to emission of $NO_y$ from supersonic aircraft, *Geophys. Res. Lett.*, *21*, 2547-2550, 1994a.

Salawitch, R. J., et al., The diurnal variation of hydrogen, nitrogen, and chlorine radicals: Implications for the heterogeneous production of $HNO_2$, *Geophys. Res. Lett.*, *21*, 2551-2554, 1994b.

Schauffler, S. M., L. E. Heidt, W. H. Pollock, T. M. Gilpin, J. F. Vedder, S. Solomon, R. A. Lueb, and E. L. Atlas, Measurements of halogenated organic compounds near the tropical tropopause, *Geophys. Res. Lett.*, *20*, 2567-2570, 1993.

Scott S. G., T. P. Bui, K. R. Chan, and S. W. Bowen, The meteorological measurement system on the NASA ER-2 aircraft, *J. Atmos. Oceanic Tech.*, *7*, 525-540, 1990.

Solomon, S., R. R. Garcia, F. S. Rowland, and D. J. Wuebbles, On the depletion of Antarctic ozone, *Nature*, *321*, 755-758, 1986.

Stimpfle, R. M., et al., The response of ClO radical concentrations to variations in $NO_2$ radical concentrations in the lower stratosphere, *Geophys. Res. Lett.*, *21*, 2543-2546, 1994.

Stolarski, R. S., et al., 1995 Scientific assessment of the atmospheric effects of stratospheric aircraft, *NASA Ref. Publ. 1381*, Washington, D. C., 1995.

Tolbert, M. A., M. J. Rossi, and D. M. Golden, Heterogeneous interactions of $ClONO_2$, HCl, and $HNO_3$ with sulfuric acid surfaces at stratospheric temperature, *Geophys. Res. Lett.*, *15*, 851-854, 1988.

Toon, O., et al., Heterogeneous reaction probabilities, solubilities, and the physical state of cold volcanic aerosols, *Science*, *261*, 1136-1140, 1993.

Van Doren, J. M., L. R. Watson, P. Davidovits, D. R. Worsnop, M. S. Zahniser, and C. E. Kolb, Uptake of $N_2O_5$ and $HNO_3$ by aqueous sulfuric acid droplets, *J. Phys. Chem.*, *95*, 1684-1689, 1991.

Webster, C. R., $NO_2$/NO partitioning as a test of stratospheric ClO concentrations over Antarctica, *Geophys. Res. Lett.*, *14*, 704-706, 1987.

Wennberg, P. O., et al., Removal of stratospheric $O_3$ by radicals: In situ measurements of OH, $HO_2$, HO, $NO_2$, ClO, and BrO, *Science*, *266*, 398-404, 1994.

Wennberg, P. O., T. F. Hanisco, R. C. Cohen, R. M. Stimpfle, L. B. Lapson, and J. G. Anderson, In situ measurements of OH and $HO_2$ in the upper troposphere and stratosphere, *J. Atmos. Sci.*, *52*, 3413-3420, 1995.

Wilson, J. C., et al., In situ observations of aerosol and chlorine monoxide after the 1991 eruption of Mount Pinatubo: Effects of reactions on sulfate aerosol, *Science*, *261*, 1140-1143, 1993.

Woodbridge, E. L., et al., Estimates of total organic and inorganic chlorine in the lower stratosphere from in situ and flask measurements during AASE II, *J. Geophys. Res.*, *100*, 3057-3064, 1995.

L. A. Del Negro, S. G. Donnelly, D. W. Fahey, R. S. Gao, (corresponding author), E. R. Keim, M. H. Proffitt, and R. C. Wamsley, 325 Broadway, R/E/AL6, Aeronomy Laboratory, National Oceanic and Atmospheric Administration, Boulder, CO 80303..

R. J. Salawitch, Jet Propulsion Laboratory, Pasadena, CA 91109.

D. E. Anderson, R. Demajistre, and S. A. Lloyd, Applied Physics Laboratory, Johns Hopkins University, Laurel, MD 20723-6099.

C. T. McElroy, Atmospheric Environment Service/Canada, Downsview, Ontario, Canada M3H 5T4.

E. L. Woodbridge, Scripps Institution of Oceanography, University of California at San Diego, La Jolla, CA 92093.

R. M. Stimpfle and D. W. Kohn, Department of Chemistry, Harvard University, Cambridge, MA 02138.

S. R. Kawa and L. R. Lait, NASA Goddard Space Flight Center, Greenbelt, MD 20771.

K. R. Chan, M. Loewenstein, and J. R. Podolske, NASA Ames Research Center, Moffett Field, CA 94035.

J. E. Dye, Mesoscale and Microscale Meteorology Division, National Center for Atmospheric Research, Boulder, CO 80307.

J. C. Wilson, Department of Engineering, University of Denver, Denver, CO 80208.

(Received October 4, 1995; revised June 18, 1996;
accepted June 18, 1996.)